Cell Reports
Physical Science

CellPress
OPEN ACCESS

Article

Chip-scale solar thermal electrical power generation

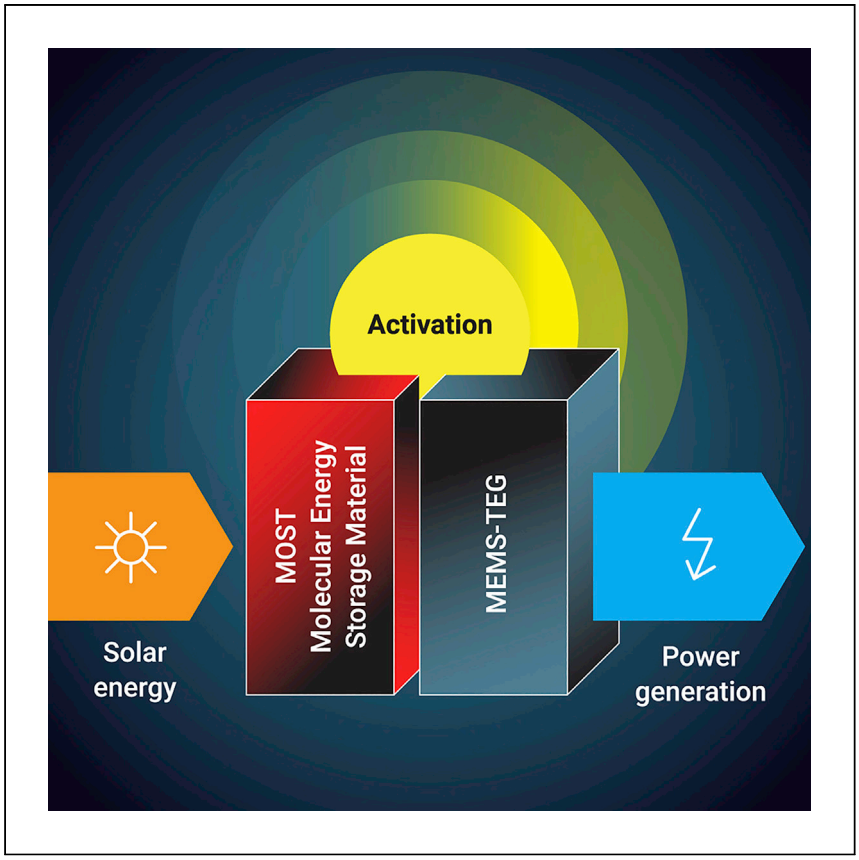

Molecular solar thermal energy storage is a technology based on photoswitchable materials, which allow sunlight to be stored and released as chemical energy on demand. Wang et al. demonstrate a molecular thermal power generation system that stores solar energy and converts it to electric power on demand.

Zhihang Wang, Zhenhua Wu, Zhiyu Hu, ..., Fengdan Wang, Tao Li, Kasper Moth-Poulsen

zhiyuhu@sjtu.edu.cn (Z.H.)
litao1983@sjtu.edu.cn (T.L.)
kasper.moth-poulsen@chalmers.se (K.M.-P.)

Highlights

Solar energy storage and conversion to electrical power generation is demonstrated

Continuous power output can be generated from the combined device

Photophysical properties of two photoswitches are fully characterized

A microelectromechanical ultrathin thermoelectric chip is designed and fabricated

Wang et al., Cell Reports Physical Science 3, 100789
March 16, 2022
https://doi.org/10.1016/j.xcrp.2022.100789

Cell Reports
Physical Science

CellPress
OPEN ACCESS

Article

Chip-scale solar thermal electrical power generation

Zhihang Wang,[1] Zhenhua Wu,[2] Zhiyu Hu,[2,*] Jessica Orrego-Hernández,[1] Erzhen Mu,[3] Zhao-Yang Zhang,[4] Martyn Jevric,[1] Yang Liu,[2] Xuecheng Fu,[5] Fengdan Wang,[5] Tao Li,[4,*] and Kasper Moth-Poulsen[1,6,7,8,*]

SUMMARY

There is an urgent need for alternative compact technologies that can derive and store energy from the sun, especially the large amount of solar heat that is not effectively used for power generation. Here, we report a combination of solution- and neat-film-based molecular solar thermal (MOST) systems, where solar energy can be stored as chemical energy and released as heat, with microfabricated thermoelectric generators to produce electricity when solar radiation is not available. The photophysical properties of two MOST couples are characterized both in liquid with a catalytical cycling setup and in a phase-interconvertible neat film. Their suitable photophysical properties let us combine them individually with a microelectromechanical ultrathin thermoelectric chip to use the stored solar energy for electrical power generation. The generator can produce, as a proof of concept, a power output of up to 0.1 nW (power output per unit volume up to 1.3 W m^{-3}). Our results demonstrate that such a molecular thermal power generation system has a high potential to store and transfer solar power into electricity and is thus potentially independent of geographical restrictions.

INTRODUCTION

From the Industrial Revolution to 2018, the global average temperature increased by 1°C as a result of human activities and may hit 1.5°C as early as 2030, as warned by the United Nations Intergovernmental Panel on Climate Change (IPCC).[1] People have been actively looking for a technology that can slow down or reduce the rise in global temperature. As the global population increases, total worldwide energy use from all sectors is expected to reach 21 TWy by 2040, corresponding to an increase of 130% over 2019 levels.[2] Electricity is an essential commodity in modern society, and around 3 TW is currently used. To complicate matters, about 85% of this power is derived from fossil fuels.[3] Therefore, searching for new decarbonized energy sources to reduce greenhouse gas emissions is imminent. Nuclear energy is a low-carbon energy source, but its installations are complex, and their thermal pollution can potentially be serious. As the most common renewable energy at present, hydropower is geographically limited, while wind energy fluctuates with season or time.[4] It is noteworthy that solar energy is the most abundant energy resource on Earth, and maximizing the use of solar power can potentially meet the intensive demand for power while reducing detrimental effects to the environment.[5] For instance, an estimated 2.3×10^4 TWy of solar power reaches Earth each year, which equates to only 7 h of sunlight needed to meet current annual global energy requirements.[6,7]

[1]Department of Chemistry and Chemical Engineering, Chalmers University of Technology, 41296 Gothenburg, Sweden

[2]National Key Laboratory of Science and Technology on Micro-Nano Fabrication, Shanghai Jiao Tong University, Shanghai 200240, China

[3]School of Materials Science and Engineering, Henan Polytechnic University, Jiaozuo 454003, Henan, China

[4]Shanghai Key Laboratory of Electrical Insulation and Thermal Aging, School of Chemistry and Chemical Engineering, Shanghai Jiao Tong University, Shanghai 200240, China

[5]Center for Advanced Electronic, Materials and Devices (AEMD) of Shanghai Jiao Tong University, Shanghai 200240, China

[6]Institute of Materials Science of Barcelona, ICMAB-CSIC, 08193 Bellaterra, Barcelona, Spain

[7]Catalan Institution for Research and Advanced Studies ICREA, Pg. Lluís Companys 23, Barcelona, Spain

[8]Lead contact

*Correspondence: zhiyuhu@sjtu.edu.cn (Z.H.), litao1983@sjtu.edu.cn (T.L.), kasper.moth-poulsen@chalmers.se (K.M.-P.)

https://doi.org/10.1016/j.xcrp.2022.100789

Photovoltaic (PV) cells can directly convert solar energy into electrical power with a maximum efficiency of around 30%, and most of the solar energy is not only lost as heat but also contributes to deteriorating the performance.[8–11] In addition, solar intensity naturally varies with time and geographical location and these variations currently limit the utilization of PV. Obviously, PV cells do not produce power during the night. Solar thermal power plants with phase-change molten salts can generate power for several hours after sunset; however, these plants require very large solar concentrators and consequently can be installed only in remote areas.[12,13] Previously, solar actuators based on hydrogen-bonded azopolymers for electricity generation have been investigated; however, the device cannot store solar energy for later on-demand power generation.[14] Hence, in addition to the above mainstream technologies, there is an urgent need for new alternative compact technologies that can derive and store energy from the sun, especially the large amount of solar heat that is not effectively used for future power generation. In this paper, we demonstrate a compact, chip-based device that allows for direct storage of solar energy as chemical energy that is released in the form of heat on demand and then converted into electrical energy in a controlled way.

To explore ways to store solar energy, we are investigating a class of materials that can capture sunlight via reversible photochemical reactions and later release this stored energy on demand. These materials operate in a closed cycle, and they use photochromic chemical compounds to form the basis of molecular solar thermal (MOST) energy storage systems.[15–18] Upon exposure to sunlight, a suitable MOST material (in the parent state) can photoisomerize to a high-energy metastable photoisomer that can be stored for extended periods of time. Depending on the photochrome used, the back-conversion reaction releasing heat energy can be triggered through different processes, including thermal,[19,20] catalytic,[21,22] electrocatalytic,[23,24] and photoinduced conversion.[25–27] It has been previously estimated that, for an ideal liquid MOST device, up to 21% of the solar energy can be stored as chemical energy for later heat production.[28] Such heat produced can be delivered locally and on demand, unlike other thermal storage technologies.

While MOST systems can be used in closed-cycle devices for efficient storage and release of heat, additional engineering is necessary to generate electrical power. Thermoelectric generators (TEGs) are able to directly convert thermal energy into electrical power via the Seebeck effect. TEGs have been widely used in various applications due to their attractive features such as silent operation, minimal maintenance, and long lifetime. And they have been considered as promising alternatives to meet the urgent demand for energy around the world.[29,30] Traditional solar thermal-to-electric power generation systems use heat engines to convert heat into electricity in two steps (heat to mechanical movements and then mechanical energy to electrical power generation).[31,32] However, a large amount of heat can be lost during the conversion process. To solve this issue, bulk TEGs have been combined with phase-change materials for power generation to convert heat to electricity directly.[31,33] Recently, low-dimensional material-based microelectromechanical system (MEMS) technology has enabled the production of ultrathin and highly sensitive TEG devices that can integrate large arrays of thermoelectric (TE) modules.[34] From our previous results, we explored a reliable and efficient hybrid method for ultrathin MEMS-TEG fabrication, and achieved up to 46,000 TE modules on a 3-in silicon wafer.[35,36] Such a MEMS-TEG equipped with an 800-nm-thin TE film has shown a steady electrical output, which was sensitive to small temperature differences and could effectively utilize low-grade thermal energy.[37] The temperatures accessible by the energy release reaction of the MOST are, at the current stage of

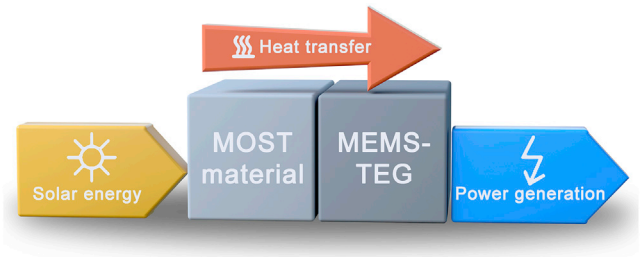

Scheme 1. Schematic illustration of the MOST to power generation concept

development, less than 100°C, which is not high enough to be utilized for electrical power generation by traditional means. Therefore, it is necessary to match the MOST systems with high-efficiency and sensitive TE devices to effectively utilize this relatively low-grade thermal energy.

Here, we design a compact, chip-based device that combines two different MOST systems operating either in the liquid or in the solid state with a novel designed MEMS-TEG to demonstrate the storage of solar energy to the release of heat energy and the cascading energy flow to the harvester that is finally used to generate power (see Scheme 1). Two molecular photoswitches with suitable properties—a norbornadiene derivative (NBD) investigated as a solution and a phase-interconvertible arylazopyrazole derivative (AZO) measured as a neat film—are selected for their potential to produce heat energy for electrical generation. The ultrathin MEMS-TEG with 572 TE modules is designed and fabricated, in which the TE films are only 1 μm thick. We characterize and couple each of these photoswitches individually with the MEMS-TEG chip (effective thermoelectricity area 10 × 6 mm), demonstrating that chemical energy stored in MOST systems (in Sweden) can successfully generate electrical power (in China) through the process of solar energy storage, heat release, and TE conversion, thus affirming that solar energy can generate electrical power independent of time and geographical restrictions.

RESULTS AND DISCUSSION

Solar energy storage properties

MOST systems can function in both liquid and film forms, which can be tailored toward different applications.[21,38–45] In liquid form, MOST systems can transport stored energy, meaning that energy can be stored and released in two different locations, whereas in film form, MOST systems can be used in smart windows and other device integrations.[43,46] In this study, we selected and tested two systems: an NBD in liquid form (in toluene solution, which can provide a low specific-heat capacity of ca. 1.6 J $g^{-1}\cdot°C^{-1}$) and a neat AZO in thin films with suitable energy capture and storage functionality. The molecular structures of both photoswitch couples are shown in Figure 1A. The photoconversion of NBD proceeds via a [2 + 2π] cycloaddition reaction to its corresponding photoisomer quadricyclane derivative (QC). Thus, the energy storage density $\Delta H_{storage}$ was experimentally determined to be 93 kJ mol^{-1} (0.37 MJ kg^{-1}). Meanwhile, QC has a thermal back conversion half-life of 1 month at room temperature, demonstrating the possibility for long-term storage in toluene. Spectroscopically, we previously showed that norbornadiene with a push-pull system has a spectral red-shifting effect on the absorption.[21] Hence, this NBD with dimethoxy donor units exhibits an absorption feature around 340 nm with a maximum absorptivity of $\varepsilon_{max@340\ nm} = 1.4 \times 10^4\ M^{-1}\ cm^{-1}$. In contrast, the absorption profile of QC is virtually negligible above 300 nm, leaving a transparent optical window of around 85 nm between both forms due to the selected push-pull substituents (see Figure 1B). This significant spectral

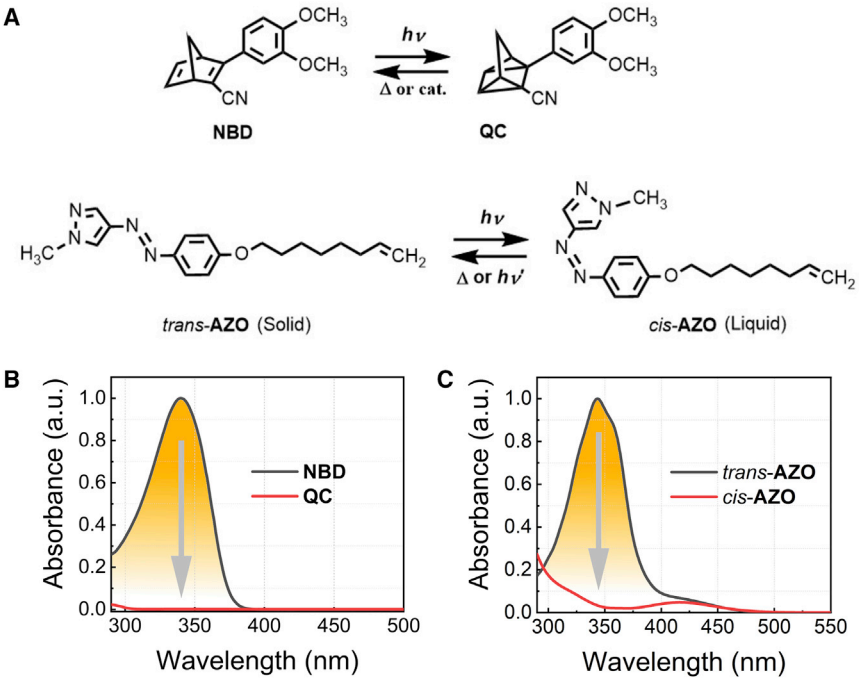

Figure 1. Structures and absorption spectra of the two MOST candidates used in this work

(A) Molecular structures of NBD-QC couple (top) and *trans*/*cis*-AZO photoswitch couple (bottom). A thermal (Δ) or catalytic (cat.) route can facilitate the back conversion of QC → NBD. The back conversion of *cis*- → *trans*-AZO can be achieved by a thermal or light-induced activation.

(B) Absorption profile of NBD before and after irradiation with 340-nm light (in toluene).

(C) Absorption profile of AZO photoswitch before and after irradiation with 365-nm light (in acetonitrile).

difference enables near-quantitative photoconversion, even in concentrated solutions. In addition, the photoisomerization quantum yield was 68% in toluene. Considering the above-mentioned MOST properties, solar energy storage efficiency of the system could exceed 0.70%[38] (see Note S1 for details).

Neat-film thermal storage devices have several attractive features, such as simple device integration and no need for mechanical pumping. Further, systems that combine energy input from solar irradiation with absorption of ambient heat have recently emerged.[46–55] Such systems couple a phase-change event to the photoconversion process found in MOST systems. One example is the AZO explored here (see Figure 1A). To take advantage of the exothermic process not only from the photoisomerization reaction but also from an additional phase-change process (liquid → crystal), we investigated the AZO photoswitch in its neat form. The energy stored in *cis*-AZO was easily released by triggering heat release following irradiation with a 532-nm light source (this wavelength is considered *cis*-AZO's onset of absorption). As shown in Figure 1C, the absorption maximum of the *trans* isomer was 344 nm with an absorptivity of $\varepsilon_{max@340\ nm} = 2.9 \times 10^4\ M^{-1}\ cm^{-1}$. The *trans*-AZO has a quantum yield of only 41%, but this is considered high for other azobenzene-based photoswitches. The photoisomerization energy density ΔH_{isom} was 52 kJ mol^{-1} (0.17 MJ kg^{-1}). In addition to heat release from the chemical reaction, the crystal-to-liquid transition (ΔH_{phase_change}) can provide an additional 50 kJ mol^{-1} (0.16 MJ kg^{-1}) of thermal energy because of its long alkenyl chain. As a result, the solar energy storage efficiency of the AZO couple was estimated to be 1.2%, which is much higher than that of other azobenzene photoswitches.[40] Moreover, *cis*-AZO is remarkably stable at room

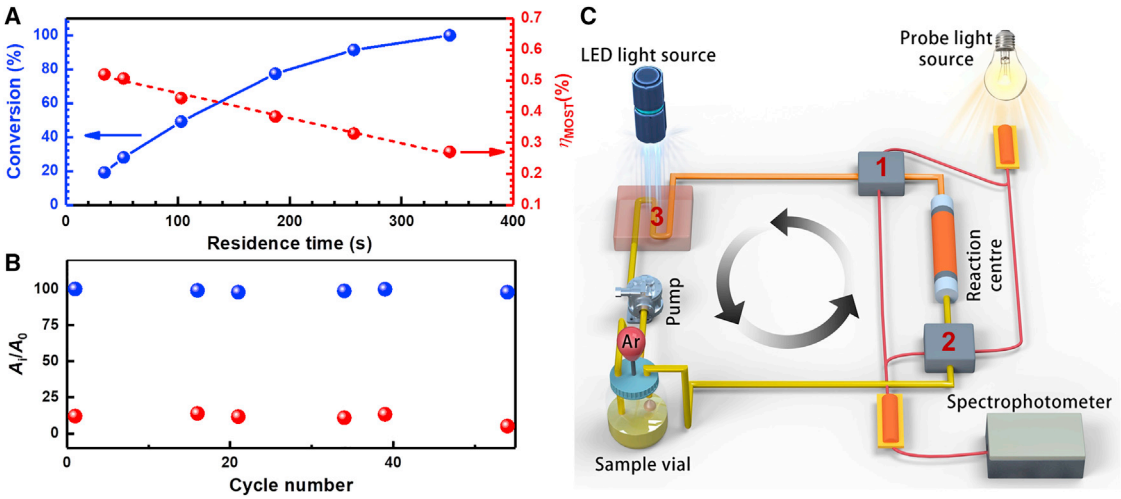

Figure 2. Conversion performance, cycling performance, and experimental setup of NBD in the device

(A) Conversion percentage (in blue) and calculated energy storage efficiency (in red) of 0.1 M NBD in toluene as a function of residence time in the device.

(B) Normalized absorbance before irradiation with 340 nm LED light and after catalytic reactor. Blue dots show the normalized absorbance at 340 nm, red dots show the normalized absorbance after irradiation.

(C) Cycling test setup for NBD. Boxes 1 and 2 represent the flow UV-vis spectrometer before and after a catalytic reaction center. Box 3 refers to the microfluidic chip. The conversion process has proceeded with irradiation from a 340 nm LED lamp.

temperature, with a thermal half-life of 3 months at 25°C. Thus, using this photoswitch from a neat film would allow two different sources of stored energy to be used: thermal ambient energy and light.[46,47]

Photoconversion in the device under various exposure times and complete interconversion through multiple cycles are important tests for photoswitch viability in a MOST system. These experimental factors have previously been reported for AZO[46] but not for NBD. Therefore, additional experiments were necessary to determine the compatibility of the NBD photoswitch. A custom-made 400-mm^2 microfluidic reactor was used for this photoconversion experiment (see Note S2 and Figure S1 for details). A solution of 0.1 M NBD (25 g L^{-1}) in toluene-d_8 was pumped through the microfluidic reactor with residence times from 34 to 343 s. The degree of photoconversion was monitored immediately afterward by ^{1}H NMR spectroscopy. For an ideal MOST system, where the absorption of the photoisomer (QC) does not compete with the absorption of the parent (NBD), the energy storage efficiency, η_{MOST}, should remain approximately unchanged prior to full conversion.[40,45,56] Here, we observed a decrease in solar energy storage efficiency from ≈0.5% at short residence times to 0.25% at full conversion. While not ideal, it is normal for efficiency to lower progressively during the conversion process. In this context, this system is better than our previous attempts at flow conversion (see Figure 2A and Note S3 for details).[21]

Typically, for cyclability testing, solution-based photoswitches are irradiated at elevated temperatures.[21,45] However, this method seemed impractical as QC has a long half-life ($t_{1/2}$≈29 days) in toluene. To address this, an alternate protocol was employed, which hastened the time frame for each successive cycle. Cobalt(II) phthalocyanine is physisorbed on activated carbon (CoPc@C) and can rapidly facilitate the back reaction of a very similar quadricyclane structure.[21] This new setup involved converting and back converting an NBD solution (0.5 mM in toluene) continuously through a microfluidic photoreactor and a catalytic reactor in a closed

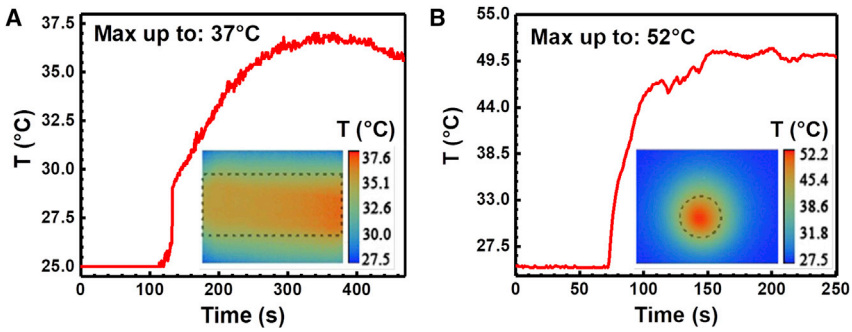

Figure 3. Macroscopic heat-release performance of QC and *cis*-AZO under infrared camera

(A) Recorded temperature increment of QC heat release over time; inset shows the thermal image from the heat-releasing copper device. The area indicated by the dashed line represents the device position.

(B) Recorded temperature increment of the *cis*-AZO system over time; inset shows the thermal image from the heat-releasing *cis*-AZO sample. The dashed line represents the position of the compound (maximum temperature gradient of 17°C after the heat generated from the laser is subtracted).

cycle. Happily, no obvious drop in performance was observed after 54 charge and discharge cycles on the NBD couple (see Figures 2B and 2C and Note S4 for details). This setup drastically reduced the total experimental time to only 61 h.

Stored energy release for NBD and AZO

Once solar energy is stored as QC and *cis*-AZO, one should be able to release the chemical energy from these metastable compounds as heat. However, we performed simulations to determine how much energy could be extracted from these charged materials. To achieve this, a simulation of possible temperature increases based on molecular parameters was performed. In the case of QC, the maximum temperature increase depended on the concentration of initial NBD in toluene. Based on the highest possible concentration of 0.78 M in toluene, the maximum estimated temperature difference under adiabatic conditions was 40°C (see Note S5 and Figure S2 for details).

To test the experiment in practice, we designed a fixed-bed catalytic heat-release device consisting of a copper tube flanked on two sides with copper plates to maximize heat transfer to the MEMS-TEG device (see Note S6 and Figure S3 for details). By taking advantage of the mobile nature of the QC solution, a heterogeneous CoPc@C catalyst[21] was loaded inside the copper tube, and a thermally conductive pad was used to provide a homogeneous thermal distribution from the tube to all areas of the device. A saturated NBD solution was initially photoconverted to QC and then pumped through the reactor at a flow speed of 5 mL h^{-1}. This speed leads to complete back conversion from QC to NBD and a maximum surface temperature of 37°C (≈13°C maximum temperature gradient, see Figure 3A and Video S1 for details). A thermal camera recorded liquid-QC macroscopic heat release, determined by the camera focusing on the top of the device.

Concerning the *trans*/*cis*-AZO photoswitch couple, the charged *cis* isomer releases 0.17 MJ kg^{-1}, equating to a simulated thermal difference of 84°C. From here, an additional 0.16 MJ kg^{-1} can be extracted at the crystallization point of the *trans*-AZO (melting point 83°C) from the phase-change event. Thus, *cis*-AZO theoretically shows a larger potential thermal gradient than the QC solution. In this case, the experimental measurement of the heat release involved the placement of a droplet of liquid *cis*-AZO (≈8 mg) under ambient conditions onto a glass substrate

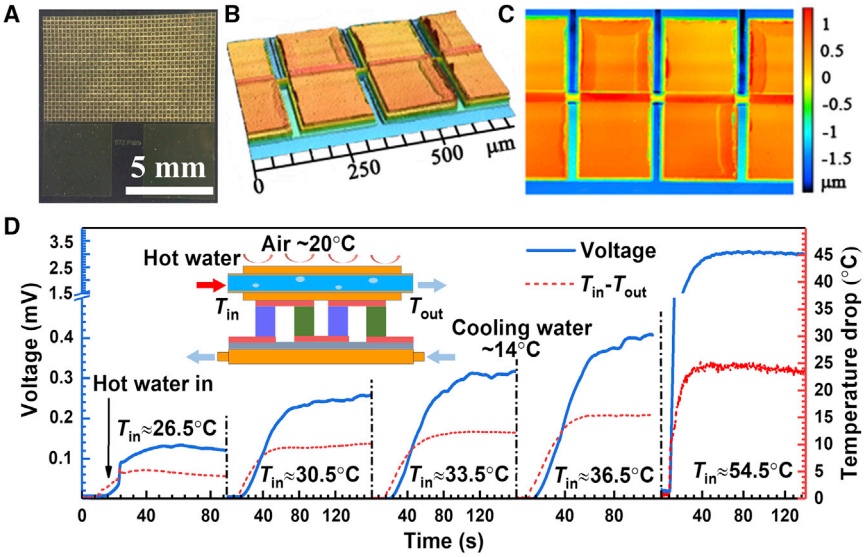

Figure 4. Thermal performance of MEMS-TEG used in this work

(A) Optical microscope photo of MEMS-TEG with 572 TE modules.

(B) Three-dimensional laser scanning confocal microscope images of the fabricated thermoelectric pairs.

(C) Top view of the fabricated thermoelectric pairs by laser scanning confocal microscopy. Scale bar shows the relative height of the device.

(D) Power generation of MEMS-TEG when hot water of different temperature flows through the copper tube at the hot end of the TEG.

(1 × 0.7 cm). A 532 nm laser was used to irradiate the sample and trigger the heat release in conjunction with a thermal camera. This triggered a full back conversion, affording a maximum surface temperature of 52°C, corresponding to a 17°C maximum temperature difference after accounting for heat from the laser. The large difference in temperature gradient between theoretical and experimental values is likely due to the strong heat dissipation from the thin film under ambient conditions (see Figure 3B and Video S2 for details). The thermal camera recorded the *cis*-AZO film macroscopic heat release.

These results showed that both solution-based NBD and neat AZO photoswitches can successfully generate heat. Next, we wanted to use this thermal energy by converting it to electrical power using the MEMS-TEG device.

Single-layered microelectromechanical thermoelectric chip

Theoretically, the figures of merit (ZT_{ave}) of low-dimensional TE materials are higher than those of bulk TE materials and can potentially yield a higher TE conversion efficiency.[57] Thin-film-based TE devices are also sensitive to small temperature differences.[35] Such technology can be used to monitor local thermal variations at micro-nano scales, such as bioactivity in yeast cultures.[58] On the other hand, if the number of integrated TE modules is high enough, the output electrical power can be significantly increased.[59] To effectively convert the heat released from MOST systems to electrical power, a large array integrated MEMS-TEG based on Bi_2Te_3 (n type) and Sb_2Te_3 (p type) TE modules was fabricated. The unit structure is designed in a Π shape, with a resistance of 72.8 Ω and a single p/n surface area of 200 × 200 μm. The fabrication process and structure diagram of the MEMS-TEG device are shown in Note S7, Figures S4–S9, and Table S1. In total, 572 TE modules were connected in series, where the height of each TE column was increased to ~1 μm with the aim of improving the TE performance at low temperature gradients,

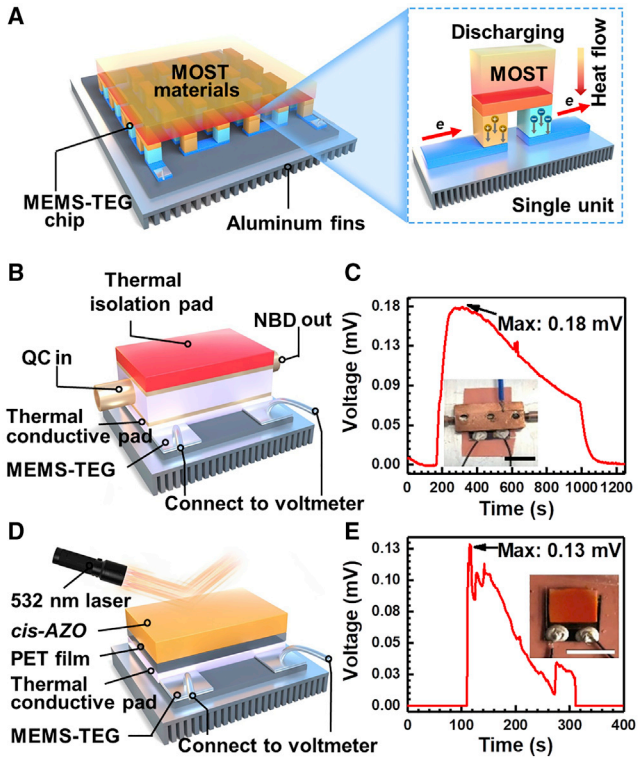

Figure 5. MOST to power generation performance

(A) Schematic concept of MOST to power generation.

(B) NBD couple-based solar energy storage for power-generation experimental setup.

(C) Heat release monitoring by thermocouple and voltage generated from MEMS-TEG chip over time. The inset is a photo of the device. Scale bar, 1 cm.

(D) Schematic experimental setup of AZO film-based solar energy for power generation.

(E) Net voltage generated from MEMS-TEG chip over time. The inset is a photo of the device. Scale bar, 1 cm.

as shown in Figure 4.[37] Most importantly, the thickness of the whole working part from the chip did not exceed 2 μm. This ultrathin structure (thickness of top contact layer of only ~300 nm and a mass of only a few picograms) responded effectively to small variations in temperature. The structure and properties of the TE materials constituting the MEMS-TEG and the power generation performance of the device are shown in Table S1 and Figures S5–S8. Since the heat released by QC in the copper tube does not cover all the tubes uniformly, as shown in Figure 3, a reference experiment was conducted to investigate the power generation of the MEMS-TEG by passing hot water into the copper tube at a flow speed of 73 mL h^{-1} in advance (see Figure S9). When the temperature of the inlet hot water was 36.5°C and 54.5°C, the corresponding voltages generated by the MEMS-TEG were 0.4 mV (maximum power output of density 6 W m^{-3}) and 3 mV (maximum power output of density 349 W m^{-3}), respectively. This shows that the higher the average temperature in the MOST reaction chamber, the greater the power output density can be reached.

Power generation from NBD and AZO

Based on the physical properties of NBD and AZO couples, two heat-to-power generation device concepts were put forth (see Figure 5A). For the NBD system, a saturated solution of QC in toluene was prepared in Gothenburg, Sweden, using a photochemical flow reactor (see Note S8 and Figure S10 for details) and shipped to Shanghai, China. For this experiment, 5 mg of CoPc@C was loaded inside the

catalytic reactor (inside the central copper tube), where a thermally conductive pad was used to fill the gap between copper plates in the device (see Figure 5B). The reactor was placed above the MEMS-TEG chip, and the whole setup was then placed on top of an aluminum brick heat sink, which ensured a stable ambient temperature and served as the cold side of the device. Importantly, the hot side of the system was covered with thermally insulated plastic foam to ensure that the heat generated was reflected instead of being lost to the environment. As a result, with less than 1 mL of a 0.78 M solution and a flow speed of 5 mL h^{-1}, a measured bias voltage of up to 0.18 mV was recorded. According to the MEMS-TEG chip characterization, this voltage can generate a maximum power output of ≈0.1 nW (power output density of 1.3 W m^{-3}, see Figure 5C). With the same flow speed, a continuous operating test with slightly lower concentration of 0.62 M in toluene was also performed. This successfully generated, for the first time, a total electric energy of up to 0.44 W h·m^{-3} over 24 min (see Note S9 and Figure S11).

In the case of AZO, a smaller amount of material was used; 7 mg of *cis*-AZO, generated from a 365 nm LED light source, was loaded onto the thermally conductive pad. A polyethylene terephthalate (PET) film was gently pressed on top of the material to allow it to fully cover the surface of the MEMS-TEG chip evenly. Laser irradiation at 532 nm triggered the back conversion (see Figure 5D), leading to a bias output voltage of up to 0.13 mV. This corresponds to a maximum power output of 0.06 nW (power output density of 0.7 W m^{-3}) (see Note S10 and Figures S12–S15 for details). Interestingly, various peaks were observed when the voltage approached the maximum. This was likely due to the complex release of heat, which involved both photoisomerization and phase transitions (see Figure 5E). We observed that less power is generated from *cis*-AZO than from QC, although the former reached a higher surface temperature, but the temperature distribution in the latter tube is more even. Not surprisingly, this is because the amount of heat released from these two systems is markedly different: 1 mL of 0.78 M QC could produce 72.5 J, while 7 mg of *cis*-AZO could produce only 2.3 J of energy.

Here, we noticed that the maximum temperatures reached by the NBD couple and the AZO couple are 37°C and 52°C, respectively, while the corresponding voltages generated by MEMS-TEG are 0.18 and 0.13 mV, respectively. However, compared with the hot water with similar temperature, the maximum power output density generated by the NBD couple and the AZO couple is greatly reduced. It is worth noting that the hot water flowing continuously and rapidly in the copper reactor has a better thermal contact surface with the pipe wall than the discharging QC solution and *cis*-AZO film. Consequently, the hot water flowing at a temperature of 36.5°C makes the power density generated by MEMS-TEG nearly 5 times that of the QC solution with similar temperature (37°C). This demonstrates that, with the MOST materials at hand, better thermal management and TE materials may increase the power output of the next generation of devices.

To the best of our knowledge, these results show the first proof of principle that solution-based MOST and PCM-MOST systems can generate electric power. Future work should focus on red shifting the absorption band (capturing more sunlight) and increasing the temperature gradient produced by the back reaction (improving energy density). The next generation of combined devices should include a better thermal management system to avoid heat dissipation from the MOST system to the surrounding environment, thereby increasing the amount of heat energy converted to electrical power output. Based on the TE film preparation method,[60] the TE efficiency can be simulated to be over 8% at room temperature (ZT_{ave} = 2.4)

and around 29% between 0 and 100 K (ZT_{ave} = 1.0) with a temperature difference of 100°C (see Note S11 and Figure S16 for details), assuming that MOST systems can achieve this absolute temperature of 100°C, which is close to what has recently been demonstrated.[21] Producing a highly soluble photoswitch of ca. 1.5 M, accompanied by a heat release of 100 kJ mol^{-1} with a 5 mL h^{-1} flow speed, would allow the system to produce a power output of 16.7 mW (0.2 GW m^{-3}) at room temperature and 60.4 mW (0.7 GW m^{-3}) at temperatures of 0–100 K. This would be enough to power a low-power-supplied Internet of Things device on Earth or in the outer space environment.[61]

In this work, we have shown two molecular photoswitches in different physical forms (liquid-based NBD and neat AZO film) for coupling MOST systems with electrical power generation via MEMS-TEG devices. The liquid-based NBD exhibits a solar energy storage efficiency of ≈0.5% in 0.5 mM toluene, which is more efficient than photosynthesis (0.1%–0.3%).[62] NBD was also, for the first time, tested through 54 charge and discharge cycles in a continuously operating energy storage and catalyzed release cycle, and showed no sign of degradation. Alternatively, the PCM-MOST hybrid neat AZO film captures and releases energy in photochemical solid-liquid transitions, which allows the MOST system to harness energy both from sunlight and from the ambient environment, meaning that upgraded heat can be produced on demand. Comparing the two candidates, both of them can store solar energy in the visible range for over a month at room temperature. To improve the macroscopic heat-release capability, future investigation of increasing the solubility of liquid-based NBD is necessary. For neat AZO, with addition phase-change properties, the overall energy storage capacity has been greatly improved. However, due to the light-induced back-conversion property of AZO, for future real-world-conditions device design, it is necessary to add a band-pass filter that is able to filter out the photons that initiate back conversion of AZO.

To demonstrate generation of power from the MOST system, an ultrathin-film-based, highly sensitive MEMS-TEG device was used to capture the heat released from either scenario. For the first time, electricity was produced in this setup, with power output up to 0.1 nW (power output per unit volume up to 1.3 W m^{-3}). Furthermore, this device continuously generated electricity, for the first time, for over 25 min. We note that this is a very compact and local solar energy storage-power generation system that operates through a mechanism entirely different from traditional PV-battery storage combinations. Furthermore, these systems can be charged and discharged across different geographic locations (Sweden to China in this work) over a few months, showing that solar energy can be stored for power generation on demand. Although the efficiency of these systems needs to be improved, we envision that they can be used in local power generation applications in the future.

EXPERIMENTAL PROCEDURES

Resource availability

Lead contact

Further information and requests for resources and procedures should be directed to the lead contact, Prof. Kasper Moth-Poulsen (kasper.moth-poulsen@chalmers.se).

Materials availability

NBD and AZO were synthesized by following the existing procedure in the literature.[38,46] All QC samples were prepared by irradiating an NBD solution with a 340 nm LED light source from Thorlabs. The conversion percentage was checked by either a ^{1}H NMR 400 MHz instrument or a Cary 60 UV-vis spectrophotometer.

CoPc@C catalyst was produced by following the existing procedure.[3] The *cis*-AZO state was prepared using a 365 nm LED light source. For photoinduced back conversion, a 532 nm laser (110 mW cm^{-2}, the beam diameter of 1.3 cm) was used to prepare the *trans*-AZO state by irradiating the *cis*-AZO sample. All solution-based spectroscopic measurements were performed in a cuvette with path length of 1 cm on a Cary 100 UV-vis spectrophotometer, scanning the wavelength from 750 to 290 nm. Absorption spectra for the outdoor test were recorded by two microflow cells and a portable spectrometer, which was purchased from Avantes. Teflon plastic tubing used was from Cole-Parmer Instrument Company.

Data and code availability

All of the data supporting the findings are presented within the article and supplemental information. All other data are available from the lead contact upon reasonable request.

SUPPLEMENTAL INFORMATION

Supplemental information can be found online at https://doi.org/10.1016/j.xcrp.2022.100789.

ACKNOWLEDGMENTS

This work was supported by the K. & A. Wallenberg Foundation, the Swedish Foundation for Strategic Research, the Swedish Research Council Formas, the Swedish Energy Agency, the European Research Council (ERC) under grant agreement CoG, PHOTHERM - 101002131, the Catalan Institute of Advanced Studies (ICREA), and the European Union's Horizon 2020 Framework Programme under grant agreement no. 951801. The MEMS-TEG chip manufacture and experimentation were supported by the National Natural Science Foundation of China (grant 51776126). The authors would like to thank the Center for Advanced Electronic Materials and Devices (AEMD) and Instrumental Analysis Center of Shanghai Jiao Tong University (SJTU) and the startup fund of Shanghai Jiao Tong University. We thank Dr. Sarah Lerch and Prof. Ben Greatrex for reading and commenting on the manuscript. We acknowledge Neuroncollective.com and Daniel Spacek for the graphical abstract.

AUTHOR CONTRIBUTIONS

Z. Wang performed all the material and MEMS-TEG chip characterizations, conversion tests, cycling tests, heat-release experiments, and power-generation demonstrations. Z. Wu carried out the MEMS-TEG chip fabrication, characterization, and TE efficiency simulation. E.M. and Z.Y.Z. performed the heat-release experiments and power-generation experiments. Y.L., X.F., and F.W. performed MEMS-TEG chip fabrication. J.O.H. performed the sample preparation with an automated flow system. M.J. and Z.Y.Z. synthesized the used compounds. Z. Wang, Z.H., T.L., and K.M.P. designed the experiments. All authors contributed to writing the manuscript.

DECLARATION OF INTERESTS

The authors declare no competing interests.

Received: November 15, 2021
Revised: January 26, 2022
Accepted: February 7, 2022
Published: March 2, 2022

REFERENCES

1. Masson-Delmotte, V., Zhai, P., Pörtner, H.O., Roberts, D., Skea, J., and Shukla, P.R. (2019). Global warming of 1.5°C (IPCC). https://www.c40.org/news/new-report-summarizes-what-the-ipcc-1-5-c-special-report-means-for-cities/?gclid=Cj0KCQiAosmPBhCPARIsAHOen-NJQIWm1dZsNt3XcdvrvXk9egKUBOOICK6huD_8R1fkSYoD3DN-nblaAsmuEALw_wcB.

2. BP plc (2019). BP statistical review of world energy, 68 edition. https://www.bp.com/content/dam/bp/business-sites/en/global/corporate/pdfs/energy-economics/statistical-review/bp-stats-review-2019-full-report.pdf.

3. Gautam, P., Kumar, S., and Lokhandwala, S. (2019). Chapter 11 - energy-aware intelligence in megacities. In Current Developments in Biotechnology and Bioengineering, S. Kumar, R. Kumar, and A. Pandey, eds. (Elsevier), pp. 211–238. https://doi.org/10.1016/B978-0-444-64083-3.00011-7. https://www.sciencedirect.com/science/article/pii/B9780444640833000117.

4. Parsons, J., Buongiorno, J., Corradini, M., and Petti, D. (2019). A fresh look at nuclear energy. Science *363*, 105. https://doi.org/10.1126/science.aaw5304.

5. Lewis, N.S., and Nocera, D.G. (2006). Powering the planet: chemical challenges in solar energy utilization. Proc. Natl. Acad. Sci. U S A *103*, 15729–15735. https://doi.org/10.1073/pnas.0603395103.

6. Perez, R., and Perez, M. (2015). IEA-SHCP-Newsletter 62, https://research.asrc.albany.edu/people/faculty/perez/Kit/pdf/a-fundamental-look-at%20the-planetary-energy-reserves.pdf.

7. Perez, R., and Perez, M. (2009). IEA-SHCP-Newsletter 50, https://www.iea-shc.org/data/sites/1/publications/2015-11-A-Fundamental-Look-at-Supply-Side-Energy-Reserves-for-the-Planet.pdf.

8. Kandeal, A.W., Thakur, A.K., Elkadeem, M.R., Elmorshedy, M.F., Ullah, Z., Sathyamurthy, R., and Sharshir, S.W. (2020). Photovoltaics performance improvement using different cooling methodologies: a state-of-art review. J. Clean. Prod. *273*, 122772. https://doi.org/10.1016/j.jclepro.2020.122772.

9. Martinho, F. (2021). Challenges for the future of tandem photovoltaics on the path to terawatt levels: a technology review. Energy Environ. Sci. *14*, 3840–3871. https://doi.org/10.1039/D1EE00540E.

10. Asefi, G., Habibollahzade, A., Ma, T., Houshfar, E., and Wang, R.Z. (2021). Thermal management of building-integrated photovoltaic/thermal systems: a comprehensive review. Sol. Energy *216*, 188–210.

11. Sobri, S., Koohi-Kamali, S., and Rahim, N.A. (2018). Solar photovoltaic generation forecasting methods: a review. Energy Convers. Manag. *156*, 459–497. https://doi.org/10.1016/j.enconman.2017.11.019.

12. Herrmann, U., Kelly, B., and Price, H. (2004). Two-tank molten salt storage for parabolic trough solar power plants. Energy *29*, 883–893. https://doi.org/10.1016/S0360-5442(03)00193-2.

13. Du, K., Calautit, J., Wang, Z., Wu, Y., and Liu, H. (2018). A review of the applications of phase change materials in cooling, heating and power generation in different temperature ranges. Appl. Energy *220*, 242–273. https://doi.org/10.1016/j.apenergy.2018.03.005.

14. Xiong, Y., Zhang, L., Weis, P., Naumov, P., and Wu, S. (2018). A solar actuator based on hydrogen-bonded azopolymers for electricity generation. J. Mater. Chem. A *6*, 3361–3366. https://doi.org/10.1039/C7TA11139H.

15. Yoshida, Z.-i. (1985). New molecular energy storage systems. J. Photochem. *29*, 27–40. https://doi.org/10.1016/0047-2670(85)87059-3.

16. Moth-Poulsen, K., Ćoso, D., Börjesson, K., Vinokurov, N., Meier, S.K., Majumdar, A., Vollhardt, K.P.C., and Segalman, R.A. (2012). Molecular solar thermal (MOST) energy storage and release system. Energy Environ. Sci. *5*, 8534–8537. https://doi.org/10.1039/C2EE22426G.

17. Kolpak, A.M., and Grossman, J.C. (2011). Azobenzene-functionalized carbon nanotubes as high-energy density solar thermal fuels. Nano Lett. *11*, 3156–3162. https://doi.org/10.1021/nl201357n.

18. Kucharski, T.J., Ferralis, N., Kolpak, A.M., Zheng, J.O., Nocera, D.G., and Grossman, J.C. (2014). Templated assembly of photoswitches significantly increases the energy-storage capacity of solar thermal fuels. Nat. Chem. *6*, 441–447. https://doi.org/10.1038/nchem.1918.

19. Bren, V.A., Dubonosov, A.D., Minkin, V.I., and Chernoivanov, V.A. (1991). Norbornadiene–quadricyclane—an effective molecular system for the storage of solar energy. Russ. Chem. Rev. *60*, 451–469. https://doi.org/10.1070/rc1991v060n05abeh001088.

20. Broman, S., Brand, S., Parker, C., Petersen, M., Tortzen, C., Kadziola, A., Kilså, K., and Nielsen, M. (2011). Optimized synthesis and detailed NMR spectroscopic characterization of the 1,8a-dihydroazulene-1,1-dicarbonitrile photoswitch. Arkivoc *2011*, 51–67. https://doi.org/10.3998/ark.5550190.0012.904.

21. Wang, Z., Roffey, A., Losantos, R., Lennartson, A., Jevric, M., Petersen, A.U., Quant, M., Dreos, A., Wen, X., Sampedro, D., et al. (2019). Macroscopic heat release in a molecular solar thermal energy storage system. Energy Environ. Sci. *12*, 187–193. https://doi.org/10.1039/C8EE01011K.

22. Cacciarini, M., Vlasceanu, A., Jevric, M., and Nielsen, M. (2017). An effective trigger for energy release of vinylheptafulvene-based solar heat batteries. Chem. Commun. *53*. https://doi.org/10.1039/C7CC01050H.

23. Brummel, O., Waidhas, F., Bauer, U., Wu, Y., Bochmann, S., Steinrück, H.-P., Papp, C., Bachmann, J., and Libuda, J. (2017). Photochemical energy storage and electrochemically triggered energy release in the norbornadiene–quadricyclane system: UV photochemistry and IR spectroelectrochemistry in a combined experiment. J. Phys. Chem. Lett. *8*, 2819–2825. https://doi.org/10.1021/acs.jpclett.7b00995.

24. Waidhas, F., Jevric, M., Bosch, M., Yang, T., Franz, E., Liu, Z., Bachmann, J., Moth-Poulsen, K., Brummel, O., and Libuda, J. (2020). Electrochemically controlled energy release from a norbornadiene-based solar thermal fuel: increasing the reversibility to 99.8% using Hopg as the electrode material. J. Mater. Chem. A *8*, 15658–15664. https://doi.org/10.1039/d0ta00377h.

25. Fu, L., Yang, J., Dong, L., Yu, H., Yan, Q., Zhao, F., Zhai, F., Xu, Y., Dang, Y., Hu, W., et al. (2019). Solar thermal storage and room-temperature fast release using a uniform flexible azobenzene-grafted polynorborene film enhanced by stretching. Macromolecules *52*, 4222–4231. https://doi.org/10.1021/acs.macromol.9b00384.

26. Hu, J., Huang, S., Yu, M., and Yu, H. (2019). Flexible solar thermal fuel devices: composites of fabric and a photoliquefiable azobenzene derivative. Adv. Energy Mater. *9*, 1901363. https://doi.org/10.1002/aenm.201901363.

27. Yan, Q., Zhang, Y., Dang, Y., Feng, Y., and Feng, W. (2020). Solid-state high-power photo heat output of 4-((3,5-dimethoxyaniline)-diazenyl)-2- imidazole/graphene film for thermally controllable dual data encoding/reading. Energy Storage Mater. *24*, 662–669. https://doi.org/10.1016/j.ensm.2019.06.005.

28. Wang, Z., Moïse, H., Cacciarini, M., Nielsen, M.B., Morikawa, M.-a., Kimizuka, N., and Moth-Poulsen, K. (2021). Liquid-based multijunction molecular solar thermal energy collection device. Adv. Sci. *8*, 2103060. https://doi.org/10.1002/advs.202103060.

29. Jaziri, N., Boughamoura, A., Müller, J., Mezghani, B., Tounsi, F., and Ismail, M. (2020). A comprehensive review of thermoelectric generators: technologies and common applications. Energy Rep. *6*, 264–287. https://doi.org/10.1016/j.egyr.2019.12.011.

30. Shi, X.-L., Zou, J., and Chen, Z.-G. (2020). Advanced thermoelectric design: from materials and structures to devices. Chem. Rev. *120*, 7399–7515. https://doi.org/10.1021/acs.chemrev.0c00026.

31. Wu, Z., Zhang, S., Liu, Z., Mu, E., and Hu, Z. (2022). Thermoelectric converter: strategies from materials to device application. Nano Energy *91*, 106692. https://doi.org/10.1016/j.nanoen.2021.106692.

32. Weinstein, L.A., Loomis, J., Bhatia, B., Bierman, D.M., Wang, E.N., and Chen, G. (2015). Concentrating solar power. Chem. Rev. *115*, 12797–12838. https://doi.org/10.1021/acs.chemrev.5b00397.

33. Kraemer, D., Jie, Q., McEnaney, K., Cao, F., Liu, W., Weinstein, L.A., Loomis, J., Ren, Z., and Chen, G. (2016). Concentrating solar thermoelectric generators with a peak efficiency of 7.4%. Nat. Energy *1*, 16153. https://doi.org/10.1038/nenergy.2016.153.

34. Li, G., Fernández, J.G., Ramos, D.A.L., Barati, V., Pérez, N., Soldatov, I., Reith, H., Schierning, G., and Nielsch, K. (2018). Integrated microthermoelectric coolers with rapid

response time and high device reliability. Nat. Electron. *1*, 555–561. https://doi.org/10.1038/s41928-018-0148-3.

35. Mu, E., Wu, Z., Wu, Z., Chen, X., Liu, Y., Fu, X., and Hu, Z. (2019). A novel self-powering ultrathin TEG device based on micro/nano emitter for radiative cooling. Nano Energy *55*, 494–500. https://doi.org/10.1016/j.nanoen.2018.10.057.

36. Mu, E., Yang, G., Fu, X., Wang, F., and Hu, Z. (2018). Fabrication and characterization of ultrathin thermoelectric device for energy conversion. J. Power Sources *394*, 17–25. https://doi.org/10.1016/j.jpowsour.2018.05.031.

37. Liu, Y., Mu, E., Wu, Z., Che, Z., Sun, F., Fu, X., Wang, F., Wang, X., and Hu, Z. (2020). Ultrathin MEMS thermoelectric generator with Bi2Te3/(Pt, Au) multilayers and Sb2Te3 legs. Nano Converg. *7*, 8. https://doi.org/10.1186/s40580-020-0218-x.

38. Jevric, M., Petersen, A.U., Mansø, M., Kumar Singh, S., Wang, Z., Dreos, A., Sumby, C., Nielsen, M.B., Börjesson, K., Erhart, P., and Moth-Poulsen, K. (2018). Norbornadiene-based photoswitches with exceptional combination of solar spectrum match and long-term energy storage. Chem. Eur. J. *24*, 12767–12772. https://doi.org/10.1002/chem.201802932.

39. Dreos, A., Wang, Z., Udmark, J., Ström, A., Erhart, P., Börjesson, K., Nielsen, M.B., and Moth-Poulsen, K. (2018). Liquid norbornadiene photoswitches for solar energy storage. Adv. Energy Mater. *8*, 1703401. https://doi.org/10.1002/aenm.201703401.

40. Wang, Z., Losantos, R., Sampedro, D., Morikawa, M.-a., Börjesson, K., Kimizuka, N., and Moth-Poulsen, K. (2019). Demonstration of an azobenzene derivative based solar thermal energy storage system. J. Mater. Chem. A *7*, 15042–15047. https://doi.org/10.1039/C9TA04905C.

41. Masutani, K., Morikawa, M.-a., and Kimizuka, N. (2014). A liquid azobenzene derivative as a solvent-free solar thermal fuel. Chem. Commun. *50*, 15803–15806. https://doi.org/10.1039/C4CC07713J.

42. Quant, M., Lennartson, A., Dreos, A., Kuisma, M., Erhart, P., Börjesson, K., and Moth-Poulsen, K. (2016). Low molecular weight norbornadiene derivatives for molecular solar-thermal energy storage. Chem. Eur. J. *22*, 13265–13274. https://doi.org/10.1002/chem.201602530.

43. Petersen, A.U., Hofmann, A.I., Fillols, M., Mansø, M., Jevric, M., Wang, Z., Sumby, C.J., Müller, C., and Moth-Poulsen, K. (2019). Solar energy storage by molecular norbornadiene–quadricyclane photoswitches: polymer film devices. Adv. Sci. *6*, 1900367. https://doi.org/10.1002/advs.201900367.

44. Morikawa, M.-a., Yang, H., Ishiba, K., Masutani, K., Hui, J.K.-H., and Kimizuka, N. (2020). A liquid arylazopyrazole derivative as molecular solar thermal fuel with long-term thermal stability. Chem. Lett. *49*, 736–740. https://doi.org/10.1246/cl.200171.

45. Wang, Z., Udmark, J., Börjesson, K., Rodrigues, R., Roffey, A., Abrahamsson, M., Nielsen, M.B., and Moth-Poulsen, K. (2017). Evaluating dihydroazulene/vinylheptafulvene photoswitches for solar energy storage applications. ChemSusChem *10*, 3049–3055. https://doi.org/10.1002/cssc.201700679.

46. Zhang, Z.-Y., He, Y., Wang, Z., Xu, J., Xie, M., Tao, P., Ji, D., Moth-Poulsen, K., and Li, T. (2020). Photochemical phase transitions enable coharvesting of photon energy and ambient heat for energetic molecular solar thermal batteries that upgrade thermal energy. J. Am. Chem. Soc. *142*, 12256–12264. https://doi.org/10.1021/jacs.0c03748.

47. Zhang, Z.-Y., He, Y., Zhou, Y., Yu, C., Han, L., and Li, T. (2019). Pyrazolylazophenyl ether-based photoswitches: facile synthesis, (near-) quantitative photoconversion, long thermal half-life, easy functionalization, and versatile applications in light-responsive systems. Chem. Eur. J. *25*, 13402–13410. https://doi.org/10.1002/chem.201902897.

48. Shi, Y., Gerkman, M.A., Qiu, Q., Zhang, S., and Han, G.G.D. (2021). Sunlight-activated phase change materials for controlled heat storage and triggered release. J. Mater. Chem. A. https://doi.org/10.1039/D1TA01007G.

49. Gerkman, M.A., and Han, G.G.D. (2020). Toward controlled thermal energy storage and release in organic phase change materials. Joule. https://doi.org/10.1016/j.joule.2020.07.011.

50. Gerkman, M.A., Gibson, R.S.L., Calbo, J., Shi, Y., Fuchter, M.J., and Han, G.G.D. (2020). Arylazopyrazoles for long-term thermal energy storage and optically triggered heat release below 0°C. J. Am. Chem. Soc. *142*, 8688–8695. https://doi.org/10.1021/jacs.0c00374.

51. Han, G.G.D., Li, H., and Grossman, J.C. (2017). Optically-controlled long-term storage and release of thermal energy in phase-change materials. Nat. Commun. *8*, 1446. https://doi.org/10.1038/s41467-017-01608-y.

52. Ishiba, K., Morikawa, M.-a., Chikara, C., Yamada, T., Iwase, K., Kawakita, M., and Kimizuka, N. (2015). Photoliquefiable ionic crystals: a phase crossover approach for photon energy storage materials with functional multiplicity. Angew. Chem. Int. Ed. Engl. *54*, 1532–1536. https://doi.org/10.1002/anie.201410184.

53. Xu, X., Wu, B., Zhang, P., Xing, Y., Shi, K., Fang, W., Yu, H., and Wang, G. (2021). Arylazopyrazole-based dendrimer solar thermal fuels: stable visible light storage and controllable heat release. ACS Appl. Mater. Interfaces *13*, 22655–22663. https://doi.org/10.1021/acsami.1c05163.

54. Xu, X., Zhang, P., Wu, B., Xing, Y., Shi, K., Fang, W., Yu, H., and Wang, G. (2020). Photochromic dendrimers for photoswitched solid-to-liquid transitions and solar thermal fuels. ACS Appl. Mater. Interfaces *12*, 50135–50142. https://doi.org/10.1021/acsami.0c14160.

55. Cai, F., Song, T., Yang, B., Lv, X., Zhang, L., and Yu, H. (2021). Enhancement of solar thermal fuel by microphase separation and nanoconfinement of a block copolymer. Chem. Mater. *33*, 9750–9759. https://doi.org/10.1021/acs.chemmater.1c03644.

56. Hansen, M.H., Olsen, S.T., Sylvester-Hvid, K.O., and Mikkelsen, K.V. (2019). Simulation framework for screening of molecular solar thermal systems in the context of a hybrid device. Chem. Phys. *519*, 92–100. https://doi.org/10.1016/j.chemphys.2018.10.020.

57. Dresselhaus, M.S., Dresselhaus, G., Sun, X., Zhang, Z., Cronin, S.B., and Koga, T. (1999). Low-dimensional thermoelectric materials. Phys. Solid State *41*, 679–682. https://doi.org/10.1134/1.1130849.

58. Latorre-Pérez, A., Vilanova, C., Alcaina, J.J., and Porcar, M. (2019). Thermoelectric heat exchange and growth regulation in a continuous yeast culture. Microbiologyopen *8*, e00648. https://doi.org/10.1002/mbo3.648.

59. Han, C.-G., Qian, X., Li, Q., Deng, B., Zhu, Y., Han, Z., Zhang, W., Wang, W., Feng, S.-P., Chen, G., and Liu, W. (2020). Giant thermopower of ionic gelatin near room temperature. Science *368*, 1091–1098. https://doi.org/10.1126/science.aaz5045.

60. Venkatasubramanian, R., Siivola, E., Colpitts, T., and O'Quinn, B. (2001). Thin-film thermoelectric devices with high room-temperature figures of merit. Nature *413*, 597–602. https://doi.org/10.1038/35098012.

61. Lee, H.G., and Chang, N. (2015). Powering the IoT: storage-less and converter-less energy harvesting. In The 20th Asia and South Pacific Design Automation Conference, *19-22* (IEEE), pp. 124–129. https://doi.org/10.1109/ASPDAC.2015.7058992.

62. Scharf, H.-D., Fleischhauer, J., Leismann, H., Ressler, I., Schleker, W.-g., and Weitz, R. (1979). Criteria for the efficiency, stability, and capacity of abiotic photochemical solar energy storage systems. Angew. Chem. Int. Ed. Engl. *18*, 652–662. https://doi.org/10.1002/anie.197906521.

Cell Reports Physical Science, Volume *3*

Supplemental information

Chip-scale solar thermal electrical power generation

Zhihang Wang, Zhenhua Wu, Zhiyu Hu, Jessica Orrego-Hernández, Erzhen Mu, Zhao-Yang Zhang, Martyn Jevric, Yang Liu, Xuecheng Fu, Fengdan Wang, Tao Li, and Kasper Moth-Poulsen

Note S1. Maximum energy storage efficiency

To calculate the maximum energy storage efficiency for **NBD**(*1*) and **AZO**(*2*), meaning the efficiency of storing sunlight as chemical energy in those materials, the following equation can be addressed:

$$\eta_{MOST} = \frac{\int_0^{\lambda_{onset}} \frac{E_{AM\ 1.5}(\lambda) \cdot (1 - \mathrm{T}(\lambda, c)) \cdot \phi_{iso} \cdot \Delta \mathrm{H}_{storage}}{h\nu \cdot N_A} \cdot d\lambda}{\int E_{AM\ 1.5}(\lambda) \cdot d\lambda} \cdot 100\ \% \qquad (1)$$

Where $E_{AM\ 1.5}(\lambda)$ is the photon energy at a specific wavelength λ, T(λ,c) corresponds to the wavelength and concentration-dependent transmittance in a specific device with a specific optical pathlength. ϕ_{iso} is the unitless photoisomerization quantum yield. $\Delta H_{storage}$ is the energy storage density in g·mol^{-1}. N_A is the Avogadro's number.

Note S2. The microfluidic chip used for NBD conversion experiments

The channels are etched isotropically (wet) 100 µm deep into the substrate, i.e., the actual structures have a lateral bias of 100 µm. The total channel volume is 33.9 mm^3. A detailed scheme is showing in figure S1.

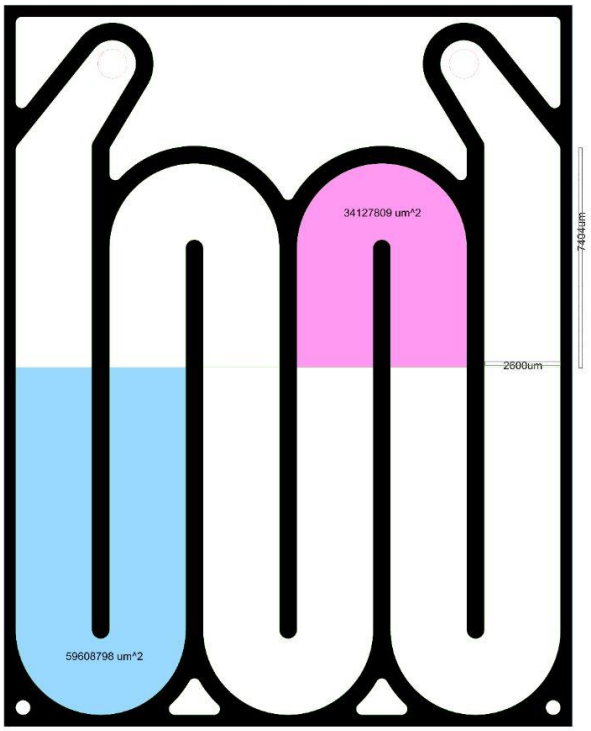

Figure S1. Customer-designed quartz chip detail.

Note S3. Energy storage efficiency during conversion experiments

During the conversion experiment, with a specific optical pathlength of the used device, the experimental energy storage efficiency can be calculated as showing below:

$$\eta_{\mathrm{MOST}} = \frac{\dot{n}_{solution} \cdot \alpha_{\mathrm{conversion}} \cdot \Delta H_{\mathrm{storage}}}{S \cdot \int E_{\mathrm{AM\ 1.5}}(\lambda) \cdot d\lambda} \quad (2)$$

Where $\dot{n}_{\mathrm{solution}}$ represents the flow speed in mol s^{-1}, $\alpha_{\mathrm{conversion}}$ corresponds to the conversion ratio from parent state to photoisomer, and S is defined as the irradiated area in m^2.

Note S4. Cycling test

Around 3 mg of CoPc@C was loaded in a plastic reaction tube, and cotton was used to block each side. **NBD** solution in toluene (4 mL, 0.5 mM) was prepared and passed through the whole setup with a speed of 50 μL/min. The conversion process has proceeded with a 340 nm LED lamp. The entire experiment for 54 cycles was run within only 61 h.

Note S5. NBD solubility and maximum heat release estimations

In a small vial with a magnetic stirring bar and 39.09 mg of NBD, 10 μL of toluene was added, and the mixture was stirred for 5 min until dissolving partially the solid. By the gradual addition of toluene (10 μL of solvent and stirring for 5 min), in the end, 220 mL of toluene was added to dissolve all the solids.

The equation below can be addressed to calculate the potential heat release from a charged photoswitchable system, and it takes the volume load factor into account:

$$\Delta T = \frac{c \cdot M_w \cdot \Delta H_{storage}}{\frac{c^2 \cdot M_w^2}{\rho_{isomer}} \cdot C_{isomer} + (1 - \frac{c \cdot M_w}{\rho_{isomer}})\rho_{solvent} \cdot C_{solvent}} \quad (3)$$

Where c and M_w refers to the concentrations of the photoswitch and molecular weight, respectively; C_{isomer} is the specific heat capacity of the material in J g^{-1} K^{-1}; $\rho_{solvent}$ and $C_{solvent}$ correspond to the volumetric mass density in g L^{-1} and the specific heat capacity in J g^{-1} K^{-1} of the solvent, respectively.

Hence, the maximum heat release estimation for **NBD** is showing in figure S2.

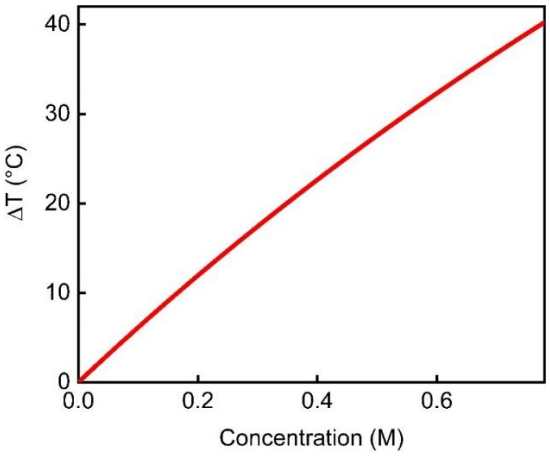

Figure S2. The maximum heat release estimation of **NBD** varied with a different concentration in toluene. For the saturated concentration of 0.78 M, the theoretical maximum ΔT can reach to 40.2°C.

Note S6. Copper catalytic reactor

For the copper catalytic reactor, a 3.5 cm copper tube with an inner diameter of 1.0 mm and an outer diameter of 2.2 mm was welded with two copper plates (1 cm x 2 cm, for later water power generation experiment, the size was reshaped as 0.6 cm x 2 cm to fit the active area of **MEMS-TEG** chip). A detailed device scheme can be found in figure S3.

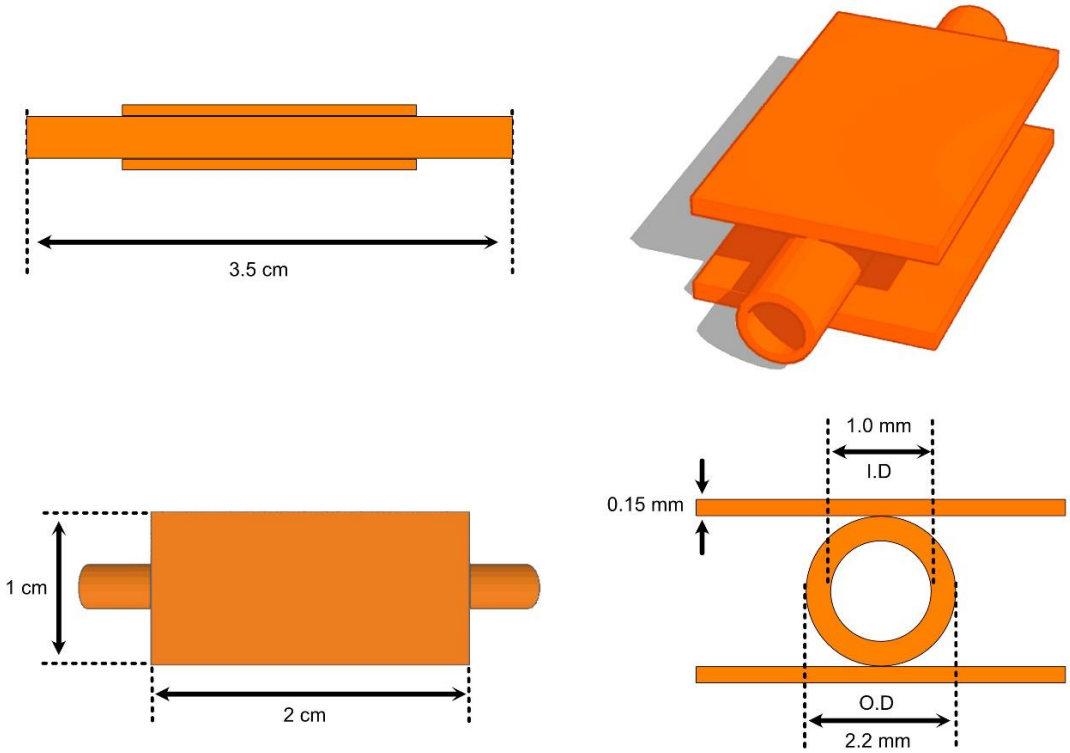

Figure S3. Scheme of the copper catalytic reactor for **QC**.

Note S7. Unit structure of the ultrathin MEMS-TEG chip

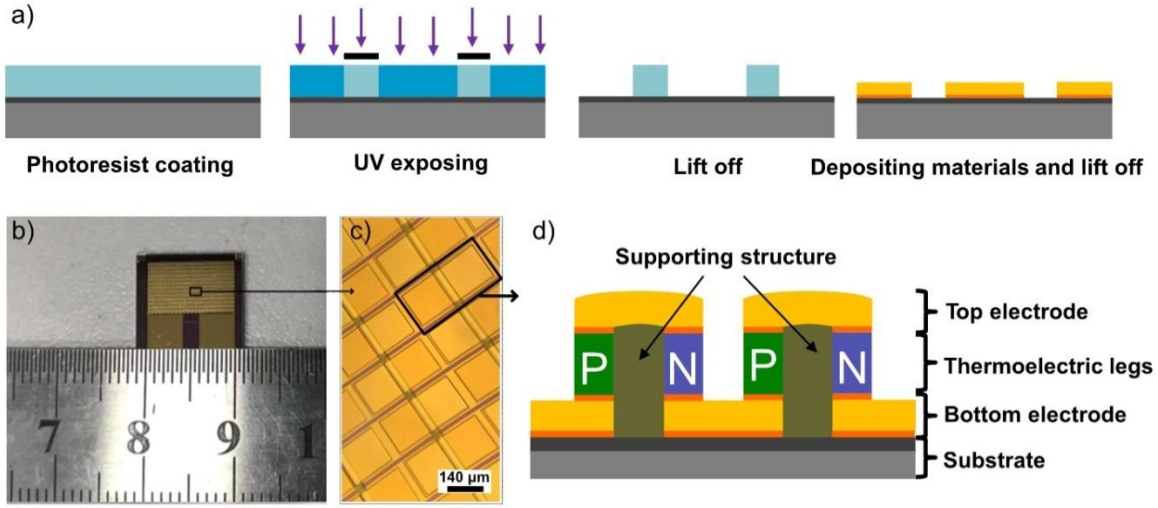

Figure S4. Fabrication and Scheme of **MEMS-TEG**.

(A) Basic steps of the fabrication for thermoelectric device, more details were proposed in our previous works(*4*, *5*).

(B) Actual **MEMS-TEG** chip picture.

(C) optical microscopic picture.

(D) schematic of ∏ shape structure. **MEMS-TEG** array of 572 TE modules have been connected in series to form the final chip. The substrate is Si covered with SiO_2 layer. The bottom electrode is Cr (20 nm) / Cu (250 nm) / Au (100 nm) / Cr (20 nm) with an area of 435 ×210 μm^2.The thermoelectric legs contains p-type Sb_2Te_3 and n-type Bi_2Te_3. The top electrode is Cr (20 nm) / Cu (250 nm) / Au (100 nm) with an area of 415×190 μm^2.

Table S1 Parameters of Sb_2Te_3 and Bi_2Te_3 thermoelectric legs

Legs	Thickness (μm)	RMS (nm)	Atomic percent (%)	
			Sb or Bi	Te

Sb_2Te_3	1.18	4.853	45.89	54.11
Bi_2Te_3	1.15	6.516	47.81	52.19

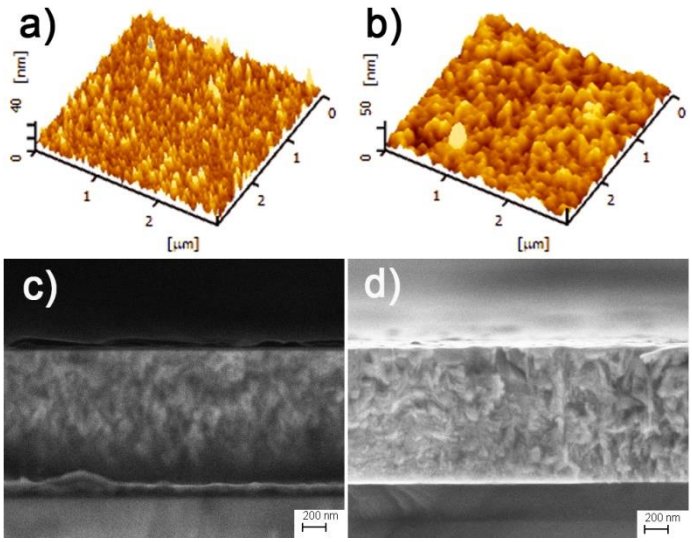

Figure S5. Topological characterizations of Sb_2Te_3 and Bi_2Te_3 thermoelectric legs.

(A) and (B) are the surface of Sb_2Te_3 and Bi_2Te_3, respectively.

(C) and (D) are the cross section of Sb_2Te_3 and Bi_2Te_3, respectively.

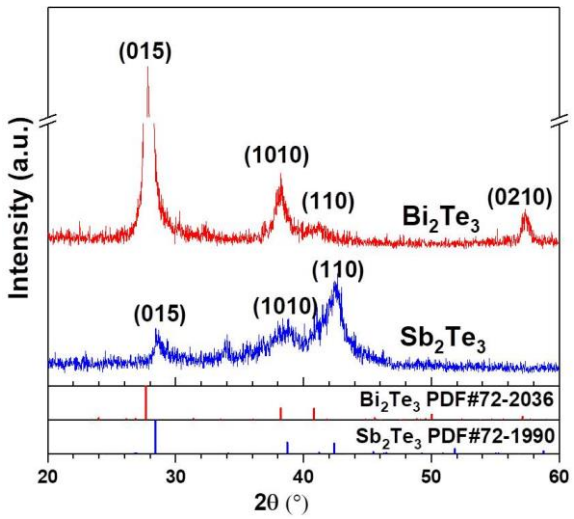

Figure S6. XRD patterns of Sb_2Te_3 and Bi_2Te_3.

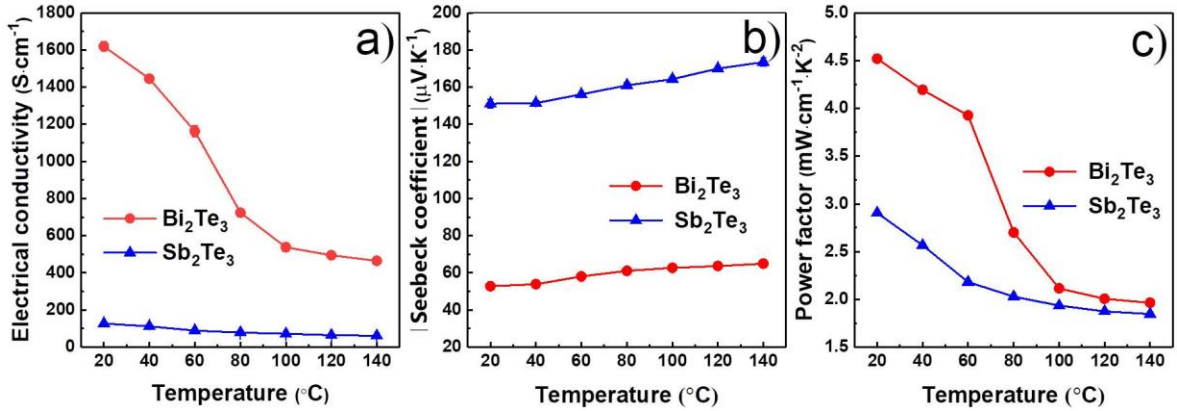

Figure S7. Experimental performance of Sb_2Te_3 and Bi_2Te_3 thermoelectric legs.

(A) Electrical conductivity measurements of Sb_2Te_3 and Bi_2Te_3 thermoelectric legs.

(B) Absolute Seebeck coefficient, positive for Sb_2Te_3 and negative for Bi_2Te_3.

(C) Power factor variation with different temperature.

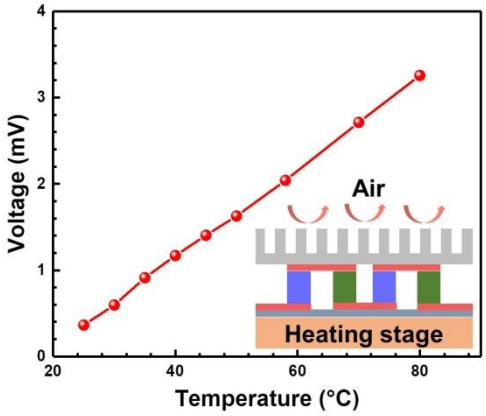

Figure S8. MEMS-TEG chip power generation varied with different heating temperature

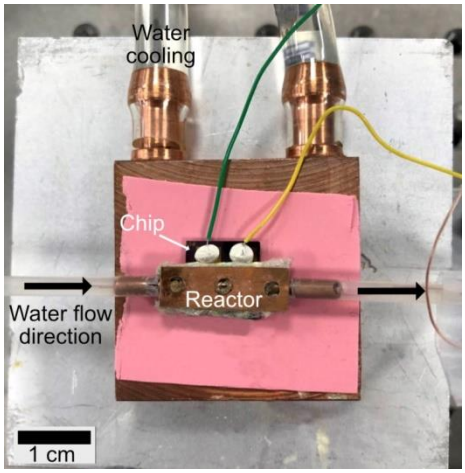

Figure S9. MEMS-TEG chip power generation setup with warm water of different temperature.

Note S8. Flow system for saturated NBD conversion experiment

A solution of **NBD** (4 mL, 0.78 M in toluene-d) was pumped at a flow rate of 0.33 mL·min^{-1} (for 30 min residence time, reactor volume: 10 mL) through the UV150 photoreactor of a Vapourtec E-series flow reactor irradiating with blue LED light (lamp power 100%, 16 watts) at 365 nm. The temperature within the reactor was controlled via a stream of chilled air, resulting in a temperature of 25–30 °C. ^{1}H NMR spectrum confirmed a 100% conversion of NBD to QC solution after passing the solution through the photoreactor. The product was then packaged and sent directly to Shanghai, China, for further experiments.

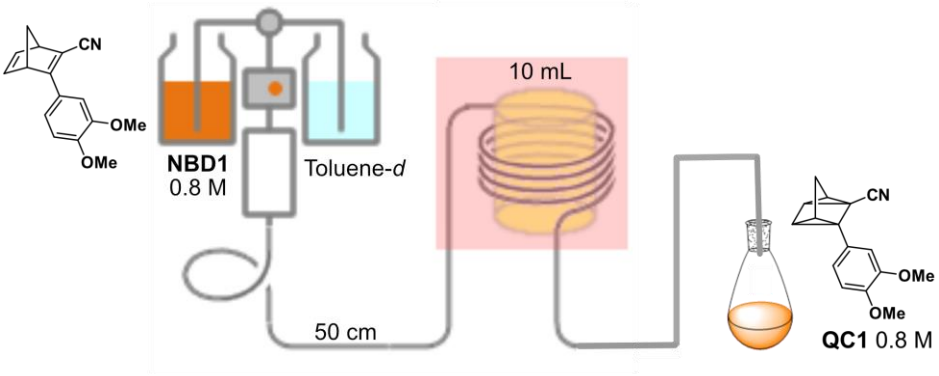

Figure S10. General Flow Reactor Configurations for the photoisomerization reaction of **NBD** to **QC**. Pink area shows the photoreactor, a residence time of 30 min was used for the conversion experiment (flow rate 0.33 mL·min^{-1}).

Note S9. Continuous operating test

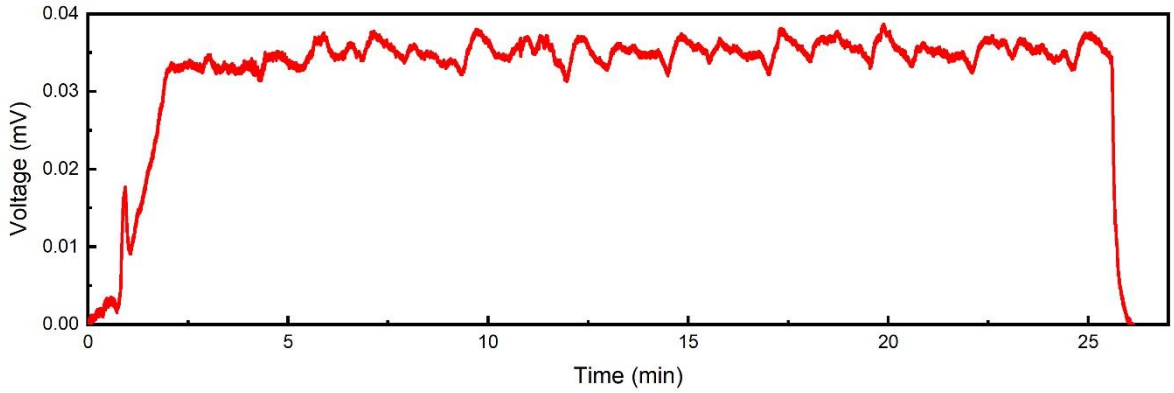

Figure S11. Continuous operating test of 0.62 M **NBD** in toluene, the electricity was successfully generated over 25 mins, produced an average electrical voltage of 0.035 mV, thus corresponds to an electric energy of 0.02 nW·h and 0.44 $W \cdot h \cdot m^{-3}$. (from 2 min to 26 min)

Note S10. NBD and AZO power generation

The macroscopic heat release experiments for each candidate **NBD** and **AZO** have been repeated three times. After each measurement, the sample was recollected for the ^{1}H NMR experiment. Full back-conversion has been confirmed for each test.

After three measurements, an average power of 0.18 mV was calculated for the **NBD** system. The different shapes of the three curves are likely due to different thermal management of the deivece in each measurements.

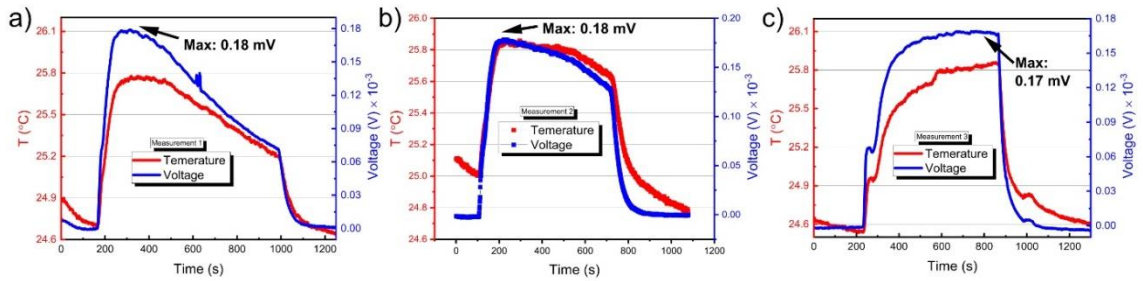

Figure S12. Three measurements (a, b, c) of voltage generation with **NBD** system.

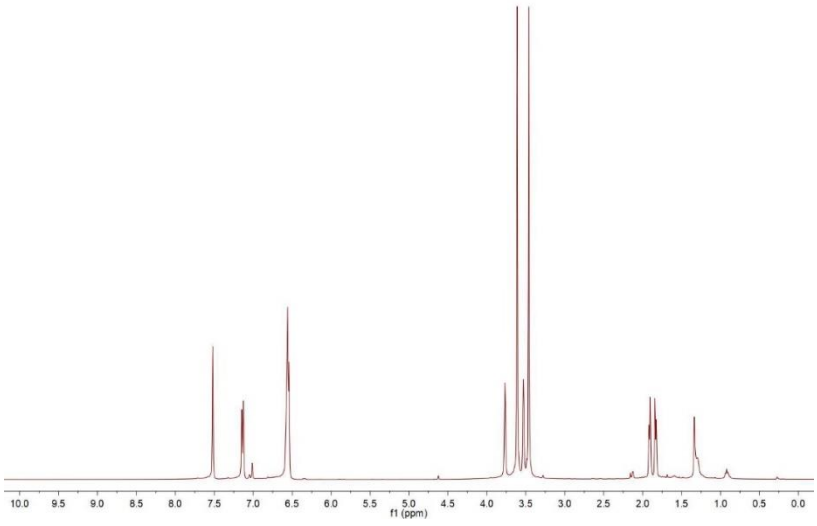

Figure S13. ^{1}H NMR of **NBD** sample after backconversion in toluene-d_8.

After three measurements, an average maximum voltage of 0.12 mV was calculated for **AZO** system. During the heat release and laser-induced crystallization, the laser was always on, and the irradiation distance was more than 10 cm. The net voltage generated by the laser (ca. 0.17 mV in three measurements) was subtracted.

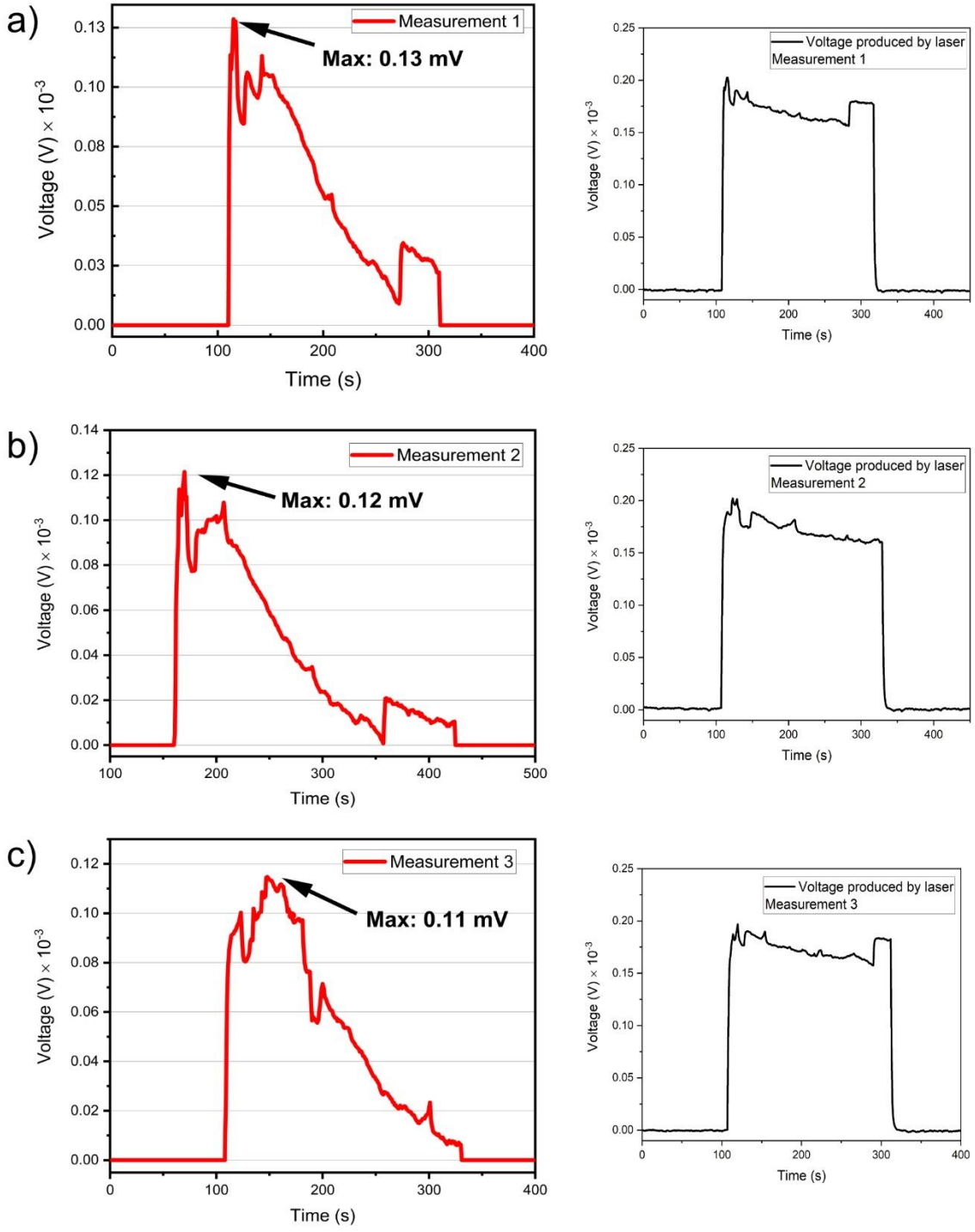

Figure S14. Three measurements of net voltage generation (a left, b left, c left) and their corresponding voltage produced by laser (a right, b right, c right) with **AZO** system.

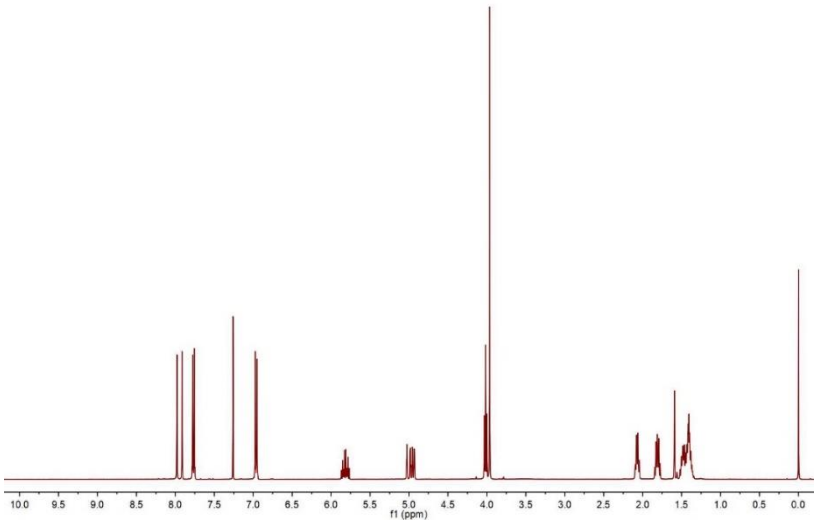

Figure S15. ^{1}H NMR of **AZO** sample after backconversion with 532 nm laser in $CDCl_3$.

Note S11. Estimation of thermoelectric efficiency

The dimensionless figure of merit, *ZT*, which helps us determine the "thermoelectric efficiency." The maximum power-generation efficiency of a thermoelectric (TE) material, η, is

$$\eta = \left(\frac{T_{hot} - T_{cold}}{T_{hot}} \right) \left[\frac{\sqrt{1+ZT_{ave}} - 1}{\sqrt{1+ZT_{ave}} + T_{cold}/T_{hot}} \right] \quad (4)$$

Where T_{cold} and T_{hot} is the temperature of the cold and hot end, respectively. ZT_{ave} is averge *ZT* between T_{cold} and T_{hot}. The average *ZT* of currently TE materials for industrial modules is between 0.5 and 1.0. The *ZT* values of the TE films in laboratories, which have excellent thermoelectric properties near room temperature, are plotted in **Figure S16a**. Based on our previously measured thermal conductivity[5], the ZT_{ave} of the Sb_2Te_3 and Bi_2Te_3 film in this work is estimated to be ~0.1. Future thermoelectric efficiency over 10% can be expected by developing materials with *ZT* values larger than 2. It is worth noting that with the same temperature gradient of 100 °C and the same *ZT* value, the thermoelectric efficiency at low temperature is superior than the high temperature as shown in **Figure S16b**.

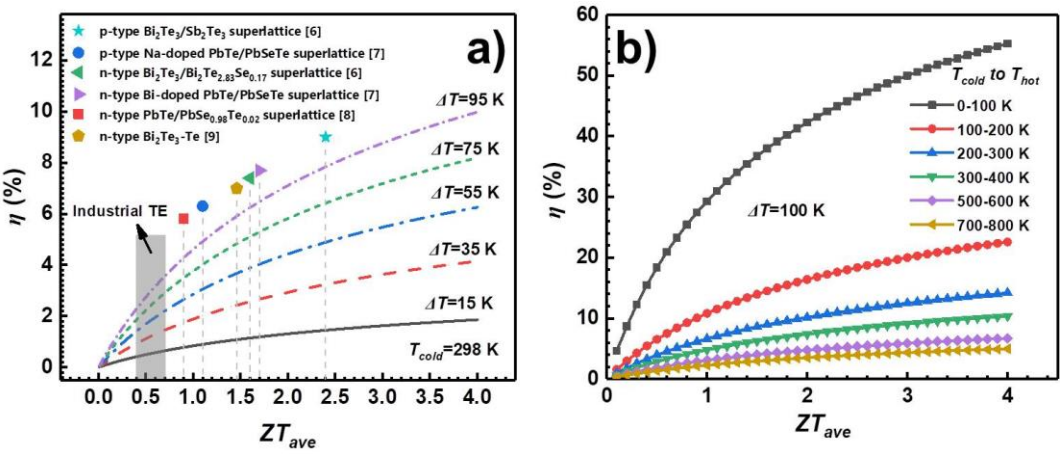

Figure S16. Theoretical estimations of the maximum power-generation efficiency with different *ZT* values.

(A) Thermoelectric efficiency with temperature differences with a cold end temperature of 298 K. The reference data in the figure is the *ZT* value at 300 K.(*6-9*)

(B) Thermoelectric efficiency varied with *ZT* at different working temperature.

Supplemental References

1. Jevric, M., Petersen, A.U., Mansø, M., Kumar Singh, S., Wang, Z., Dreos, A., Sumby, C., Nielsen, M.B., Börjesson, K., Erhart, P., and Moth-Poulsen, K. (2018). Norbornadiene-Based Photoswitches with Exceptional Combination of Solar Spectrum Match and Long-Term Energy Storage. Chem. Eur. J. *24*, 12767-12772. 10.1002/chem.201802932.

2. Zhang, Z.-Y., He, Y., Wang, Z., Xu, J., Xie, M., Tao, P., Ji, D., Moth-Poulsen, K., and Li, T. (2020). Photochemical Phase Transitions Enable Coharvesting of Photon Energy and Ambient Heat for Energetic Molecular Solar Thermal Batteries That Upgrade Thermal Energy. J. Am. Chem. Soc. *142*, 12256-12264. 10.1021/jacs.0c03748.

3. Wang, Z., Roffey, A., Losantos, R., Lennartson, A., Jevric, M., Petersen, A.U., Quant, M., Dreos, A., Wen, X., Sampedro, D., et al. (2019). Macroscopic heat release in a molecular solar thermal energy storage system. Energy Environ. Sci. *12*, 187-193. 10.1039/C8EE01011K.

4. Mu, E., Yang, G., Fu, X., Wang, F., and Hu, Z. (2018). Fabrication and characterization of ultrathin thermoelectric device for energy conversion. J. Power Sources *394*, 17-25. 10.1016/j.jpowsour.2018.05.031.

5. Liu, Y., Mu, E., Wu, Z., Che, Z., Sun, F., Fu, X., Wang, F., Wang, X., and Hu, Z. (2020). Ultrathin MEMS thermoelectric generator with Bi2Te3/(Pt, Au) multilayers and Sb2Te3 legs. Nano Converg. *7*, 8. 10.1186/s40580-020-0218-x.

6. Venkatasubramanian, R., Siivola, E., Colpitts, T., and O'quinn, B. (2001). Thin-film thermoelectric devices with high room-temperature figures of merit. Nature *413*, 597-602.

7. Harman, T., Walsh, M., and Turner, G. (2005). Nanostructured thermoelectric materials. J. Electron. Mater. *34*, L19-L22.

8. Harman, T., Taylor, P., Spears, D., and Walsh, M. (2000). Thermoelectric quantum-dot superlattices with high ZT. J. Electron. Mater. *29*, L1-L2.

9. Choi, H., Jeong, K., Chae, J., Park, H., Baeck, J., Kim, T.H., Song, J.Y., Park, J., Jeong, K.H., and Cho, M.H. (2018). Enhancement in thermoelectric properties of Te-embedded Bi2Te3 by preferential phonon scattering in heterostructure interface. Nano Energy *47*, 374-384.